AIChE WILEY InterScience DISCOVER SOMETHING GREAT

PARTICLE TECHNOLOGY AND FLUIDIZATION

In Situ WAXS Synchrotron Radiation Study on Particle Formation of Precipitated Barium Sulfate

Martin Kucher, Tobias Beierlein, and Matthias Kind
Institut für Thermische Verfahrenstechnik, Universität Karlsruhe (TH), 76128 Karlsruhe, Germany

DOI 10.1002/aic.11450
Published online February 29, 2008 in Wiley InterScience (www.interscience.wiley.com).

The particle formation process during the precipitation of barium sulfate from aqueous solutions of barium chloride and sodium sulfate was studied experimentally and numerically. Particle formation was examined offline and in situ on timescales ranging from 55 ms to 1 s. Precipitation experiments were performed in a tubular reactor of adjustable length equipped with a flow-through cuvette. The mass fraction of the crystalline precipitate was followed time-resolved using wide-angle X-ray scattering (WAXS), performed at the synchrotron radiation facility ANKA of FZK Karlsruhe GmbH. A high degree of correspondence between numerical and experimental results was achieved using nucleation kinetics based on experimental findings in combination with diffusion-controlled growth kinetics in the population balance equation. Furthermore, the online measurements showed that the lattice ion ratio (educt ratio) has no influence on nucleation kinetics, which means that the adsorption of lattice ions on pre-nuclei has no influence on their respective interfacial energy. © 2008 American Institute of Chemical Engineers *AIChE J,* 54: 1178–1188, 2008
Keywords: precipitation, particle formation, barium sulfate, X-ray scattering, population balance modeling

Introduction

Precipitation or reaction crystallization is an important industrial process. Many substances, such as fine and bulk chemicals, pharmaceuticals, biochemicals, catalysts, pigments, photographic materials, and ceramics, are produced by precipitation. Desired product properties are a defined particle size and a narrow particle size distribution, but also specific particle morphology or product crystallinity. In cases of very low solubility of the precipitated substances and for economic reasons, high supersaturations have to be used for precipitation processes. Because of these high supersaturation levels, the associated primary processes nucleation and crystal growth proceed very quickly, often on timescales below one second. These short timescales are the reason why particle formation processes during the early stages of precipitation of sparingly soluble substances are still insufficiently studied—if at all.

Precipitation of barium sulfate has been widely studied in the past decades. Numerous theoretical and experimental research studies are reported on nucleation and growth kinetics[1–4] and on the influence of reactor geometries and mixing conditions on the resulting particle size or to test precipitation models.[5–8] Most of these studies were carried out as batch or semi-batch processes, where mixing of the reactants has a dominant influence due to the very fast nucleation and growth kinetics of barium sulfate. Little attention has been paid to the pure solid formation mechanisms on short timescales without the influence of mixing.

Recent investigations have tried to cover this gap by performing experiments with fast sampling devices and Kryo-TEM investigations.[9] Based on their Kryo-TEM observations, Judat and Kind[9] proposed a new growth mechanism for barium sulfate based on ordered aggregation of nanoscale primary particles, followed by a subsequent recrystallization step. The disadvantage of this measuring technique is that

Correspondence concerning this article should be addressed to M. Kucher at martin.kucher@ciw.uka.de.

© 2008 American Institute of Chemical Engineers

only qualitative ideas on what is happening are provided and no quantitative values for the primary process kinetics can be extracted. The Kryo-TEM investigations in particular are highly sensitive with respect to sample preparation and the sample penetration with the electron beam in the microscope, which can easily lead to artifacts.

To observe the particle formation process of sparingly soluble substances, a fast, nondestructive measuring method is required, capable of measuring in a milliseconds time range. A possible approach is to use X-ray (XRD) synchrotron radiation to monitor the precipitated crystalline matter *in situ*. Different methods have been applied. One possibility of monitoring barium sulfate crystallization was shown by Hennessy et al.[10] They precipitated barium sulfate from sea brines and recorded one diffraction pattern over a time period of 20 min. Yoon et al.[11] investigated the crystallization of barium titanate nanoparticles in a glass capillary. The exposure time for one XRD data set was 60 s. Using a reaction cell, Norby et al.[12] obtained time-resolved XRD patterns at 30-s intervals during the precipitation of barium sulfate. Ueno et al.[13] studied the crystallization of a polymorphic substance in a batch crystallizer penetrated by an X-ray beam, recording diffraction data at intervals of 10 s. Heeley et al.[14] and MacCalman and Roberts[15] made online XRD measurements by continuously pumping the product suspension from a batch crystallizer through a separate measurement cell. The time resolution was 10 s. It is fairly self-evident that all experimental approaches presented above are not fast enough to monitor precipitation reactions in a time range below 1 s. Much shorter timescales can be achieved using the stopped-flow technique, where the time limitation is only given by the exposure time needed for diffraction data of sufficient quality. Bolze et al.[16] were able to study the formation mechanism of calcium carbonate with a time resolution of 100 ms using the stopped-flow method. Quayle et al.[17] studied different crystalline materials with the stopped-flow technique using time frames down to 20 ms. However, Quayle notes a big disadvantage using the stopped-flow technique if the precipitated crystals start to sediment and particles move out of the penetrating X-ray beam. To overcome the limitations associated with the exposure time, Haselhuhn et al.[18] developed a continuous-flow technique. They studied the pseudo-polymorphic behavior of precipitated calcium oxalate by means of a fast mixing device, combined with tubular reactors of different lengths connected to a flow-through cell. Using this concept, the time of precipitation is clearly defined by the length of the tube reactor and the volume flow rate of the suspension running through it. It was possible for the first time to make time-resolved observations of the particle formation process between 15 ms and 30 s. All of these studies used synchrotron radiation to provide the high photon flux necessary for short measuring times as the solids content in suspension is commonly very small in precipitation processes and it must be considered that the radiation is also absorbed by the solvent.

The aim of this study is to follow the particle formation process of a sparingly soluble substance, namely barium sulfate, with the help of online and offline measurements. In combination with the numerical description of the precipitation process based on population balance modeling, quantitative information on the temporal evolution of the primary crystallization kinetics is revealed.

Materials and Methods

Barium sulfate was precipitated from aqueous sodium sulfate and barium chloride solutions according to Eq. 1:

$$BaCl_2 + Na_2SO_4 \rightarrow BaSO_4 \downarrow + 2\,NaCl \qquad (1)$$

Stock solutions were prepared from the corresponding crystalline reagent grade solids, barium chloride dihydrate (Roth, 4453.4, pro analysis) and sodium sulfate (Merck, 1.06649.5000, pro analysis), dissolved in distilled water. All precipitation experiments were carried out at a constant temperature of 25°C as continuous experiments in a Y-mixer (Figure 1, top). The Y-mixer consists of two feed tubes of 0.5-mm diameter and an outflow tube of 2-mm diameter. Reactants were fed to the mixing device with equivolumetric flow rates of 300 ml/min, adjusted and kept constant by two PID controllers. From the Y-mixer the product suspension flows through a reaction tube of variable length.

For offline measurements, about 200 ml of suspension were collected in a beaker and analyzed 5 min after preparation. Depending on the size of the produced particles, static or dynamic light scattering was used to measure the particle size distributions (Malvern Mastersizer-S with a wet sample dispersing unit or Malvern Zetasizer 3000, respectively). Suspensions with mean particle sizes smaller than 300 nm

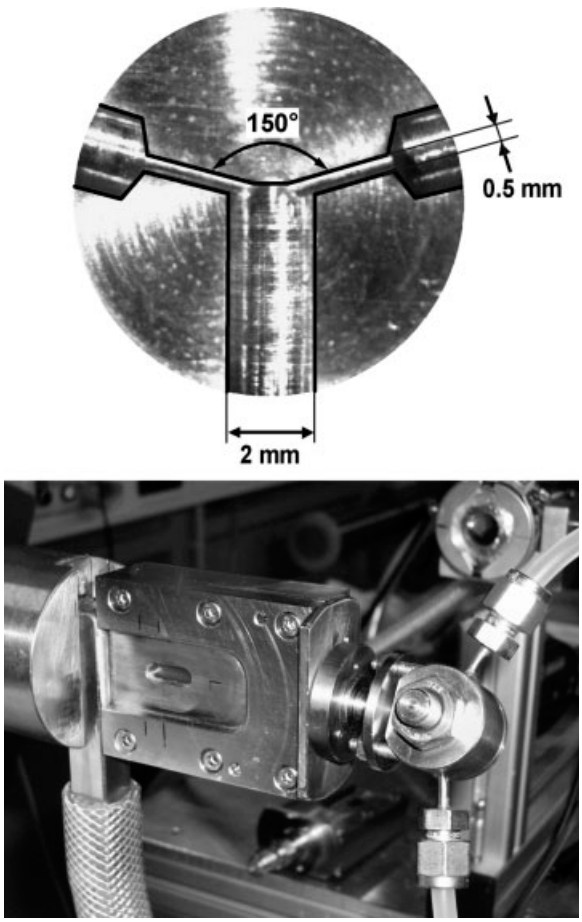

Figure 1. Interior view of Y-mixing device (top) and Y-mixer coupled with flow-through cell for shortest residence time of 55 ms (bottom).

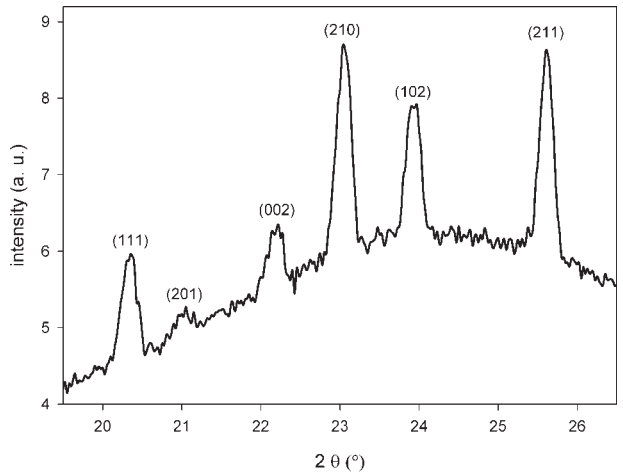

Figure 2. Diffraction pattern and characteristic Bragg peaks of barium sulfate suspension with a mass fraction of $x_{BaSO_4} = 0.015$ recorded at a X-ray wavelength of 1.38 Å.

were measured with the dynamic light scattering method. With the Y-mixer set-up as it is presented here, it was ascertained by experiment that, under the employed flow conditions, mixing should have no influence on the resulting particle size distribution and therefore on the solid formation process.[19] In addition, selected samples were analyzed by scanning and transmission electron microscopy (SEM: Leo 1530 Gemini, TEM: Philips Cm 200 Feg/St).

For the *in situ* measurements, a flow cuvette was attached to the mixer reaction tube system (Figure 1, bottom), which was already used successfully by Haselhuhn et al.[18] The cell has a path length of 1 mm and is equipped with X-ray transparent polyimide windows of 25 μm thickness. By adjusting the tube length between the Y-mixer and the flow-through cell, reaction times between 54.5 ms and 28.7 s can be realized. The flow cell was mounted in transmission geometry at the diffraction beamline of the ANKA synchrotron facility at Forschungszentrum (FZK) Karlsruhe GmbH. Detailed information on the synchrotron source and the beamline can be found in Göttlicher and Hagelstein.[20] Measurements were performed at a wavelength of 1.38 Å.

Figure 2 shows WAXS (wide angle X-ray scattering) data scattered by barium sulfate crystals in suspension. The solid mass fraction of barium sulfate was $x_{BaSO_4} = 0.015$.

The collected diffraction data clearly show the presence of crystalline material. For further investigations, the (211) peak was chosen. Exposure time for one XRD pattern, after steady-state conditions of the educt volume streams were achieved, was 200 s.

By considering the system as a two-phase system consisting of solution and barium sulfate crystals, the mass fraction of the crystalline barium sulfate phase can be calculated from the integral intensity I_{BaSO_4} of the (211) Bragg peak:

$$I_{BaSO_4} = \frac{K_{(211)BaSO_4} \cdot x_{BaSO_4}}{\rho_{BaSO_4} \cdot \mu_m} \quad (2)$$

In this equation, $K_{(211)\ BaSO_4}$ is a constant (which depends on factors such as the wavelength of the incident radiation, the cross-sectional area of the incident beam, temperature and geometry), μ_m is the mass absorption coefficient of the mixture of phases and ρ_{BaSO_4} is the bulk density of barium sulfate. For experiments with the flow-through cuvette, the constant $K_{(211)BaSO_4}$ was determined with the help of barium sulfate suspensions with defined solid contents. Several suspensions of known solid content were pumped in a loop through the measuring cell. Figure 3 shows the results of the calibration.

The quality of the calibration is excellent also due to the fact that all calibration measurements were performed in the absence of supersaturation. In the course of the experiments, it was noticed that the presence of supersaturation in the solution can lead to crystal growth on the windows of the flow-through cell. The measured intensity I_m then consists of two terms: the scattering of the crystals in suspension I_{BaSO_4}, which is the desired value and the contribution of the crystals grown on the window (I_c). To quantify the contribution of the crystals grown on the cell windows, the measured intensity has to be corrected. This was done by performing a consecutive, identical run with pure water after each measurement. The integral intensity I_c measured during this water run was subtracted from the intensity measured during the experiment (I_m):

$$I_{BaSO_4} = I_m - I_c \quad (3)$$

Figure 4 clarifies this experimental approach for the baseline-corrected (211) peak of the barium sulfate XRD pattern recorded at supersaturated conditions:

The (211) peak in the measurement as well as in the correction run was fitted with the help of *WinPLOTR* software.[21] All corrections were made under the assumption that the scattered contribution of the crystals grown on the windows is constant during the measurement as well as during the correction run. Figure 5 shows eight measurements in succession for the integral intensity measured under one supersaturated condition (upper points), which means one selected reaction time ($t = 67$ ms), followed by eight measurements with pure water for the correction term (lower points).

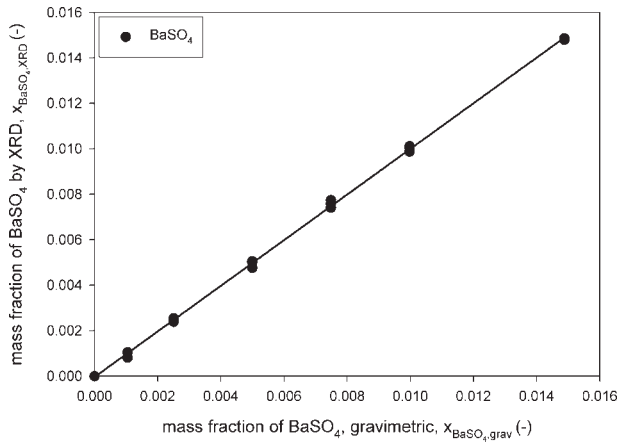

Figure 3. Mass fraction of barium sulfate in suspension, as determined by XRD synchrotron experiments versus the gravimetrically determined values.

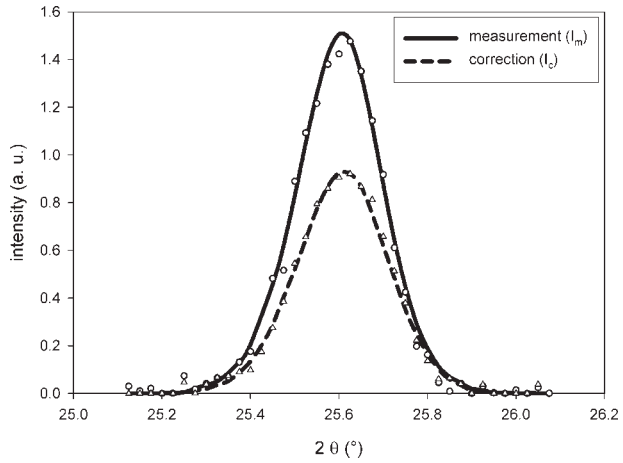

Figure 4. Examples of baseline-corrected diffraction pattern of barium sulfate in supersaturated solution and of the subsequent correction run with pure water.

Figure 5 clearly demonstrates that the above made assumption is justified. All eight measurements show about the same value of integral intensity for the measurement as well as the correction term. This means that the scattered contribution of the crystals grown on the cell windows is present and constant directly after the supersaturated solution has entered the measurement cell and the intensity does neither increase nor decrease during both runs. The increased scattering of the intensity values is due to the fact that the integration time for the XRD pattern was not the above-mentioned 200 s but had to be decreased to 80 s due to the limited volume of the educt storage tanks.

Modeling the precipitation process

The precipitation process is modeled and simulated assuming plug-flow conditions through the mixer and the reaction tube. Particles in the model are characterized by the diameter L of a volume equivalent sphere and the temporal evolution of the particle size distribution is modeled on a one-dimensional population balance equation including terms for nucleation and growth (Eq. 4).

To solve the population balance equation, the commercial software PARSIVAL by Cit GmbH was applied using the Galerkin h-p method with a time discretization of Rothe's type.

$$\frac{\partial n(L)}{\partial t} = \underbrace{B(S_a, \gamma_{cl})}_{\text{nucleation}} - \underbrace{\frac{\partial [G(S_a, L) \cdot n(L)]}{\partial L}}_{\text{growth}} \tag{4}$$

The first term on the right-hand side addresses nucleation. It comprises a kinetic expression for the nucleation rate, multiplied by a function describing the size distribution of nuclei. In this case a narrow Gaussian distribution is used as nuclei distribution, with a standard deviation of five percent of the mean size of the critical nucleus.

The secondary process aggregation is neglected in the population balance equation, based on the fact that all offline measurements of particle sizes were carried out under barium ion excess. This excess of barium ions leads to ion adsorption on the precipitated particles, creating positive charges on the particles surface that lead to repulsive electrostatic particle–particle interactions.[8,19,22] This ion excess is absolutely necessary to stabilize particles against aggregation and to obtain reliable information on the primary particles present in suspension. The validity of neglecting aggregation is confirmed by a comparison of the result of an image analysis (measuring 1000 single particles) with the result of a dynamic light scattering measurement. This was done for the highest studied supersaturation of $S_a = 1000$ at $R = 5$. Figure 6 clearly shows that, under these conditions, particles in the sub-100 nm range are produced and can clearly be identified as single particles. The particle size distributions measured by dynamic light scattering and image analysis correspond very well, demonstrating that a primary particle size distribution is obtained.

Supersaturation

The thermodynamic driving force for the primary crystallization processes nucleation and growth is supersaturation. Because of the relatively high ionic strength in supersaturated solutions (up to 0.5 mol/l in this study), ion activities instead of concentrations are used for the calculation of the supersaturation.

The activity-based supersaturation is defined as follows,

$$S_a = \sqrt{\frac{a_{Ba^{2+}_{free}} \cdot a_{SO^{2-}_{4,free}}}{K_{sp}}} = \gamma_{\pm} \sqrt{\frac{c_{Ba^{2+}_{free}} \cdot c_{SO^{2-}_{4,free}}}{K_{sp}}} \tag{5}$$

with the value of the solubility product $K_{sp} = 9.82 \cdot 10^{-11}$ mol^2/l^2 at 25 °C taken from Monnin.[23] The mean activity coefficient $\gamma_{\pm}$ can be calculated as a function of ionic strength using the semi-empirical method proposed by Bromley.[24]

The index "free" on the activities and concentrations of the ions points out that, for the calculation of the supersaturation, the activities of the "free" ions in solution have to be

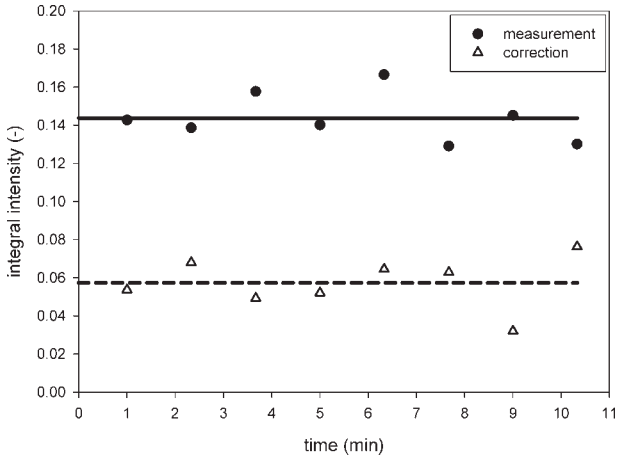

Figure 5. Integral intensity of the measurement and the correction term as a function of time for particles at one defined residence time of t = 67 ms.

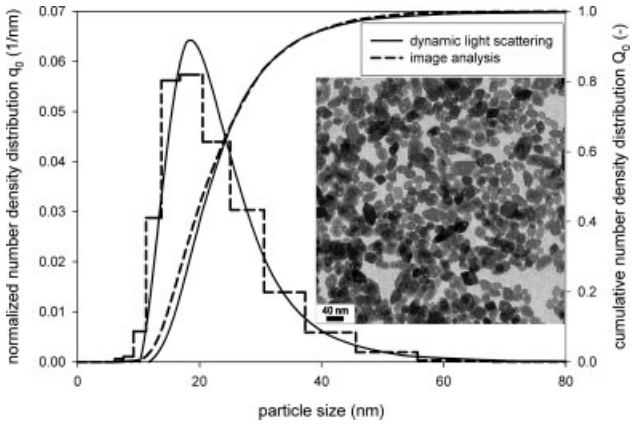

Figure 6. Comparison of particle size distributions obtained by TEM image analysis and dynamic light scattering for particles produced by a supersaturation of S_a = 1000 at R = 5; the insert shows a TEM picture of the produced nanoscale particles.

used, i.e. barium sulfate does not behave like a strong electrolyte that dissociates completely in water. Barium sulfate rather forms undissociated metal-sulfate (ion-pair) complexes $BaSO^0_{4(aq)}$, as discussed in Monnin,[23] which reduce the number of "free" barium and sulfate ions through the following reaction:

$$Ba^{2+}_{free} + SO^{2-}_{4,free} \Leftrightarrow BaSO^0_{4(aq)} \tag{6}$$

The equilibrium between complex and free ions is defined by:

$$K_{ip} = \frac{c_{Ba^{2+}_{free}} \cdot c_{SO^{2-}_{4,free}} \gamma_{\pm}{}^2}{c_{BaSO^0_{4(aq)}} \cdot \gamma_{BaSO^0_{4(aq)}}} = 5.5 \cdot 10^{-3} \frac{mol}{l} \tag{7}$$

Assuming that the value of the activity coefficient of neutral species such as ion-pair complexes is close to unity, the activity-based supersaturation S_a can be calculated.

From Eq. 5 it can be seen that a supersaturation is not necessarily created by equal free ion concentrations, i.e. under stoichiometric conditions. Therefore the free ion ratio R, which is another expression for the educt ratio of the components, is defined as:

$$R = \frac{c_{Ba^{2+}_{free}}}{c_{SO^{2-}_{4,free}}} \tag{8}$$

Nucleation

Nucleation kinetics of barium sulfate have been studied by several authors (Nielsen,[1] Mohanty et al.,[2] and Angerhöfer[3]) under stoichiometric conditions (R = 1). Although all three authors studied the same crystalline substance, namely barium sulfate, their reported experimental data and the proposed models are not very consistent (Figure 7).

All experimental data were fitted by the following nucleation rate equation, for the heterogeneous and homogeneous region respectively:

$$J_{het/hom} = J_{max,het/hom} \cdot e^{\left(-\frac{A_{het/hom}}{\ln^2 S_a}\right)} \tag{9}$$

$J_{max,het/hom}$ [m^{-3} s^{-1}] and $A_{het/hom}$ [-] are kinetic parameters and have to be adapted to the experimental data. Additionally, the parameter A_{hom} in the exponent can be expressed as a function of bulk properties,

$$A_{hom} = \frac{16\pi\ V_m^2\ \gamma_{cl}^3}{3(k_B T)^3} \tag{10}$$

i.e. $V_m = 8.95 \cdot 10^{-29}$ m^3, the molecular volume (calculated from the molar mass and the bulk density of barium sulfate) and the interfacial energy γ_{cl}. The size of the critical nucleus L_c, to estimate the distribution of nuclei in the population balance equation, was calculated using the following equation taken from Mersmann[25]:

$$L_c = \frac{4\gamma_{cl} V_m}{\nu k_B T \ln S_a} \tag{11}$$

The fitting of the experimental nucleation rate data was done by using the original data of the above mentioned authors. The quantity to describe the driving force of the precipitation process, used to present the nucleation data in the original literature—concentrations in the case of Nielsen,[1] concentration-based supersaturation in the case of Mohanty et al.[2] and Angerhöfer[3]—was recalculated to an activity-based supersaturation S_a as it was defined in the previous section.

Although all experimental data are presented well by Eq. (9) (lines in Figure 7), with different parameters for J_{max}, and A, for the heterogeneous and the homogeneous nucleation region respectively (see Table 1), it is clear that there are great differences and uncertainties between the three authors. The interfacial energy was only recalculated for the homogeneous nucleation region.

(a) The kinetic parameters as well as the nucleation rates differ by orders of magnitude between the data measured by Nielsen[1] and Mohanty et al.,[2] although in their experiments the same range of supersaturation was investigated.

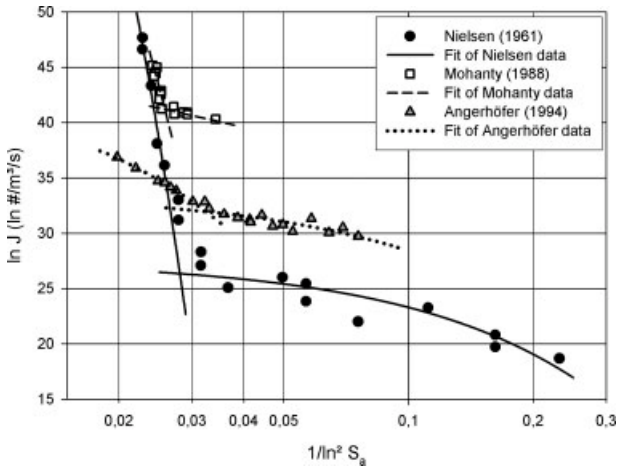

Figure 7. Nucleation rates of barium sulfate measured by different authors.

Table 1. Fitted Kinetic Parameters, Critical Supersaturation and Recalculated Interfacial Energy for Nucleation Rate Data, Measured by Different Authors

	Heterogeneous		Homogeneous			
Author	A_{het}	$J_{max,het}$ $m^{-3}\cdot s^{-1}$	$S_{a,krit}$	A_{hom}	$J_{max,hom}$ $m^{-3}\cdot s^{-1}$	γ_{cl} $J\cdot m^{-2}$
Nielsen[1]	42.35	$9.13\cdot10^{11}$	391	3943.36	$3.25\cdot10^{59}$	0.1299
Mohanty et al.[2]	109.22	$1.33\cdot10^{19}$	498	2473.58	$3.72\cdot10^{45}$	0.1112
Angerhöfer[3]	39.69	$1.94\cdot10^{14}$	237	381.15	$1.77\cdot10^{19}$	0.0596

(b) The slopes of the logarithmic nucleation rates, particularly in the homogeneous nucleation region, vary significantly, resulting in different interfacial energies γ_{cl}.

(c) All authors present different values for the so-called critical supersaturation $S_{a,crit}$, which is the value at which the change from the heterogeneous to the homogeneous nucleation region occurs.

A similar comparison of measured nucleation rates, not only for barium sulfate, was made by Roelands et al.[26] Furthermore, Roelands discusses the fact that the use of concentration-based (S_c) instead of activity-based (S_a) supersaturations will lead to different slopes in the nucleation data fits, resulting in different values for the interfacial energy. With the activity-based supersaturation model used in this study, Roelands's thesis can not be supported by the authors. Based on the nucleation data measured by Nielsen,[1] it was found here that the use of S_a or S_c has only a negligible influence on the resulting interfacial energies γ_{cl}. Using only the data of the homogenous region, the difference in γ_{cl} was less than 2%. Such a high degree of correspondence is probably due to the fact that all nucleation experiments were performed under stoichiometric conditions. However, it should be noted that the use of activity-based supersaturation becomes much more significant under non-stoichiometric conditions ($R \neq 1$).

Different nucleation kinetics were tested to describe the particle formation process of barium sulfate and will be discussed in the results and discussion section.

Crystal growth

Crystal growth can usually be considered as a two-step process: the diffusional transport of building units to the surface and the integration of these units into the crystal lattice. As is the case for all consecutive processes, it is the slower of the two that is the rate-controlling step, i.e. the one that determines the overall kinetics.

The growth of barium sulfate can be considered as diffusion- or transport-controlled at high supersaturations, which is experimentally supported by the findings of Nielsen[27] and Angerhöfer et al.[3] Both authors obtained the change in growth rate from integration- to diffusion-limited growth at supersaturations between $S_a \approx 38 - 40$. The supersaturations investigated as part of this study are considerably higher, between $S_a \approx 250 - 1000$; therefore integration-controlled growth is neglected. Therefore, the kinetic expression for growth rate is given by, i.e., see[8]:

$$G = Sh_{min} \cdot \frac{2D_{BaSO4}V_m}{L} \cdot \sqrt{K_{sp}} \cdot (S_a - 1) \qquad (12)$$

This linear growth rate, which mainly depends on particle size and supersaturation, was derived for spherical particles based on the mass transport equation. The mass transfer coefficient can be calculated by setting the Sherwood number to $Sh_{min} = 2$. This is valid under the assumption that there is no motion between particles and surrounding fluid, which is true for particles of a diameter L smaller than 10 μm.[28] The diffusion coefficient $D_{BaSO_4} = 1.1 \cdot 10^{-9}$ m^2/s is calculated using the Stokes-Einstein equation.

Results and Discussion

Offline measurements

As discussed in a previous section, the initial free ion ratio was set to $R = 5$ to avoid any effect of aggregation. Figure 8a–d shows scanning electron microscopy (SEM) and transmissions electron microscopy (TEM) pictures of particles produced at three different supersaturations between $S_a = 250$ and $S_a = 1000$, with an initial free ion ratio of $R = 5$. The particles produced at the highest supersaturation of $S_a = 1000$, $R = 5$ were already presented in the insert of Figure 6 and are again shown in Figure 8d).

All crystals shown in Figure 8a–d are single crystals, which was confirmed by electron diffraction in a TEM. Especially the crystals in Figure 8b, c look more like aggregates than single crystals, but the visible surface structures are not the result of aggregated primary particles, but are attributed to a high degree of dendritic crystal growth. This leads to a very rough and furrowed crystal surface. At a low supersaturation of $S_a = 250$, particles with a plate-like base and platelets growing out of the base plate are found. Well-defined edges and corners are observed. Increasing supersaturation to $S_a = 500$, crystal size changes only slightly, but particle morphology is greatly affected. The edges of the crystals become more rounded, rough and imperfect, clearly showing dendritic growth structures. This is due to the fact that crystal growth is faster at higher supersaturations, but the nucleation rate is only slightly increased in this supersaturation range, which means only a small increase in particle number. A further increase of supersaturation to $S_a = 600$ leads to a dramatic change to smaller particle sizes but with dendritic particle morphology still present. Now the homogeneous nucleation mechanism has taken control, leading to more and smaller particles. At an initial supersaturation value of $S_a = 1000$, the homogeneous nucleation rates are very high, leading to a huge number of particles being formed. In consequence of this high nucleation rates the primary particle sizes remain below 50 nm and therefore nanoparticles are produced.

The effect of supersaturation on measured mean (volume-weighted) particle size compared with simulation results over a wide range of supersaturation is presented in Figure 9.

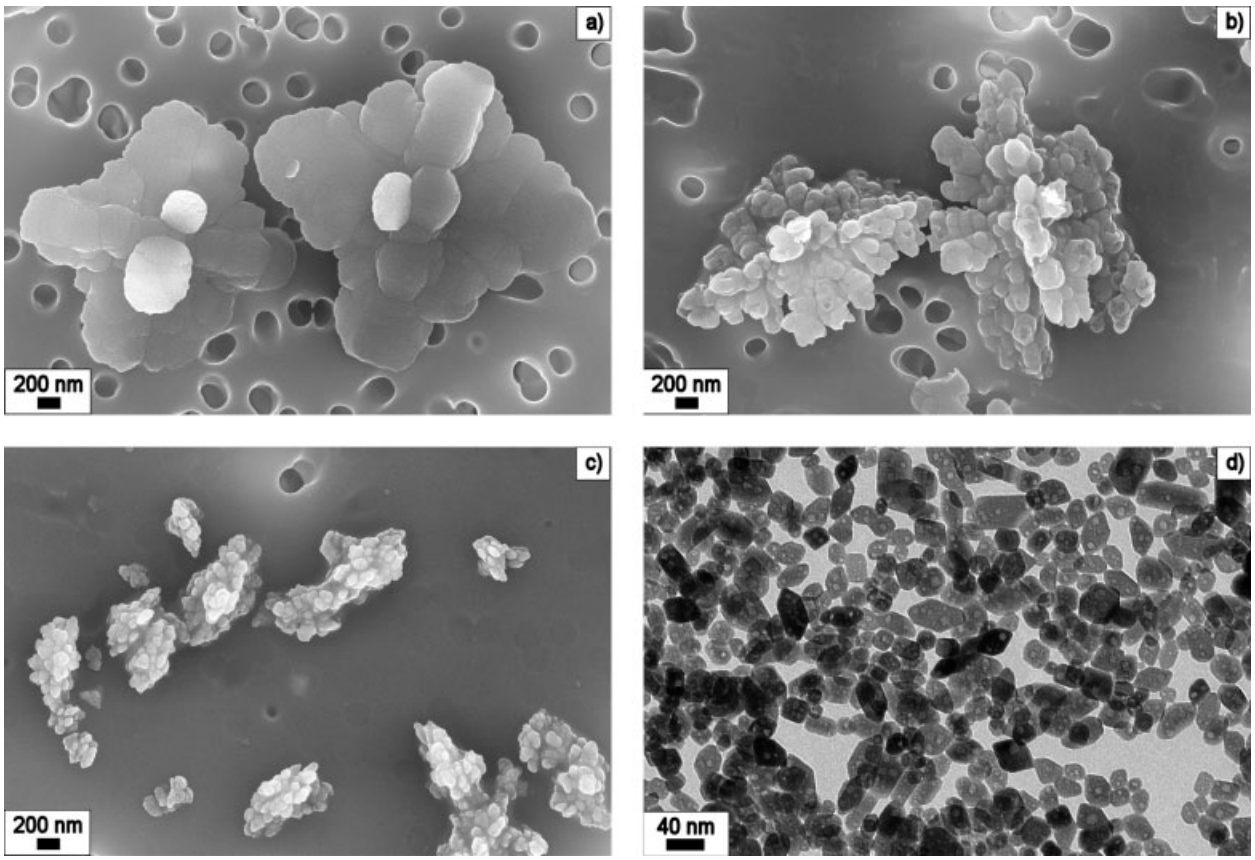

Figure 8. SEM and TEM images of precipitated barium sulfate at various supersaturations but at constant initial free lattice ion ratio $R = 5$, (a) $S_a = 250$, (b) $S_a = 500$, (c) $S_a = 600$, (d) $S_a = 1000$.

Initial supersaturation was varied between S_a-values of 250 and 1000. Two regions can be identified in the diagram: on the left-hand side the particle size remains almost constant, with increasing supersaturation between S_a = 250–550. This is the region of heterogeneous nucleation with increasing supersaturation, more heterogeneous nuclei are activated, leading to the formation of more particles. On the other hand, as supersaturation is increased, a larger amount of mass is brought into the system and deposited on this increased number of particles. The result of these two contrary working effects is an almost constant final particle size. If the critical supersaturation is crossed ($S_a >$ 550), homogeneous nucleation is the dominant nucleation mechanism, which leads to a continuously decreasing particle size with increasing supersaturation.[19]

As can be seen in Figure 9, using fitted nucleation data measured by Nielsen[1] for the heterogeneous and the homogeneous region (solid line), a good qualitative correspondence between simulation and experiment is already achieved. It is remarkable that in the heterogeneous region in particular, the simulation overestimates the mean particle size, although fewer particles are created by this nucleation mechanism and nucleation takes place on a more moderate timescale in comparison to the homogeneous nucleation region. As a result, the experimental error made by Nielsen, which inevitably results from particle counting and the measurement of induction times, should actually be smaller in the heterogeneous nucleation region.

If the nucleation data measured by Angerhöfer[3] is used, an excellent degree of correspondence is achieved between experiment and simulation. The differences between the

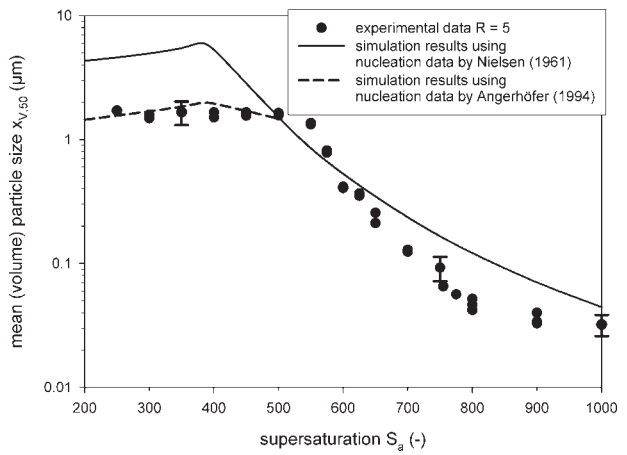

Figure 9. Comparison of experimental data precipitated under constant initial free lattice ion ratio R = 5 with simulation results using different semi-empirical nucleation kinetics combined with diffusion-controlled crystal growth.

Error bars show double the value of the standard deviation based on ten different experiments.

nucleation kinetics can be explained by the different experimental set-ups used by the two authors. Nielsen and Angerhöfer worked with a fast mixing device to reduce the influence of mixing. Both authors used counting techniques to obtain the number of particles being formed. Nielsen determined the particle number by counting particles observed in a microscope. Angerhöfer employed an automatic single particle counter working on a light-blocking principle. The difference in the experimental set-up of the two authors is revealed by the characteristic time, taken as the nucleation time for the calculation of nucleation rates. The nucleation rate is defined as the number of nuclei N emerging in a time period t_n, which is the formation time of the critical nucleus:

$$J = \frac{N}{t_n} \tag{13}$$

Nielsen optically determined the induction time t_{ind}, which represents the sum of the time necessary for the critical nucleus to be formed, t_n, and the time this nucleus needs to grow to a visible size t_g.

$$t_{ind} = t_n + t_g$$

This means that the measurements taken by Nielsen overestimate the nucleation time, resulting in the underestimation of the nucleation rate, which leads to larger particles in the simulation. Angerhöfer overcame this disadvantage using a reaction tube connected to the mixing device, which defines the time of nucleation for the crystal. As the crystals leave the tube, subsequent quenching immediately stops the primary processes by reducing the remaining supersaturation so far that equilibrium conditions are almost reached. This difference in nucleation timescale can clearly be seen in the simulation plot (dashed line). Here nucleation kinetics measured by Angerhöfer were used. A high degree of correspondence between experiment and simulation is found for the heterogeneous nucleation region, indicating that the nucleation as well as the growth kinetics reflect the correct order of magnitude and in fact seem to be the right choice. Additionally, the critical supersaturation was shifted to the left, coinciding very well with the experimentally obtained values. Unfortunately, the data obtained by Angerhöfer for the homogeneous region can not be used because the nucleation rates are way too low to produce reasonable results. Angerhöfer explains this fact with the occurrence of aggregation in the sampling beaker, with the result that only aggregates are counted instead of primary particles, leading to a strong decrease in the number of counted particles. The nucleation rate data measured by Mohanty et al.[2] is much too high to produce any reasonable simulation result. For further validation of the primary crystallization kinetics in situ, time-resolved measurements were performed.

In situ observations

All experiments described in this section were performed at an initial supersaturation of $S_a = 600$ but with different initial free lattice ion ratios R. Figure 10 shows the time-resolved evolution of the (211) peak of barium sulfate as a function of time, beginning with a time of 55 ms up to 750 ms, precipitated from an initial supersaturation of $S_a = 600$ under stoichiometric conditions ($R = 1$). Each peak consists of the actual measurement and the scattering intensity obtained by a successive water run (correction term) as discussed earlier in this study. All peaks presented in Figure 10 are baseline-corrected.

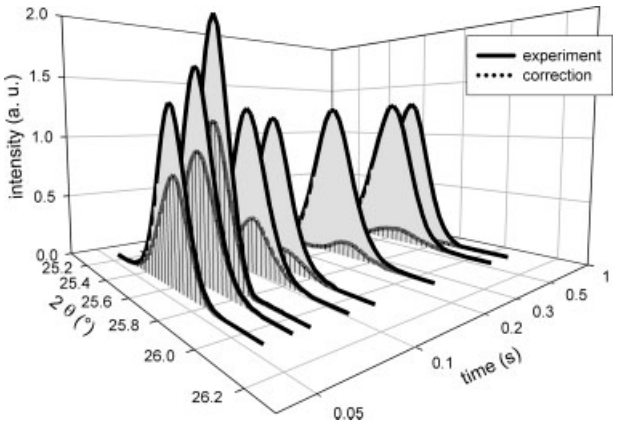

Figure 10. Time-resolved and baseline-corrected evolution of the (211) peak during precipitation from $S_a = 600$, $R = 1$, solid line: experiment, dotted line: correction term.

Across very short timescales ($t = 55$ ms–105 ms), the contribution of the correction term is very high. This indicates that across these very short timescales a high degree of supersaturation is present in the liquid surrounding the crystals. In the subsequent solids formation process, supersaturation is decreased, leading to smaller correction terms. In the case of $t = 750$ ms, no correction term was recorded due to the fact that solubility equilibrium was already reached and no incrustations on the cell windows occurred. Again, the mass present in the system is proportional to the area between the experiment and the correction curve. It is obvious that the mass in the system increases over time. In other words, Figure 10 shows the *in situ* observed evolution of a crystalline phase over time.

Using a mass balance, the actual concentration of barium and sulfate ions in solution $c_{Ba^{2+}}(t)$ and $c_{SO_4^{2-}}(t)$ can be calculated. This allows the calculation of the actual supersaturation present in solution during the precipitation process. No information from the simulations is required for this calculation. Figure 11 shows the reduction of supersaturation over time for three different initial free lattice ion ratios R, compared with simulation results using the nucleation kinetics measured by Nielsen[1] in combination with diffusion-controlled crystal growth.

The experimental data of the in situ experiments are a lot more scattered compared with the calibration results. This is certainly due to the effect of the supersaturation now present in the system. Several conclusions can be drawn from Figure 11. No major difference in supersaturation depletion results from precipitation performed under stoichiometric conditions ($R = 1$) or under barium ion excess ($R = 2, 5$). After 55 ms, the shortest reaction time for which measurements were possible, the supersaturation is already depleted. The solubility equilibrium is reached far below one second, which explains the lack of reliable kinetic data for precipitation processes at such high supersaturations in the open literature.

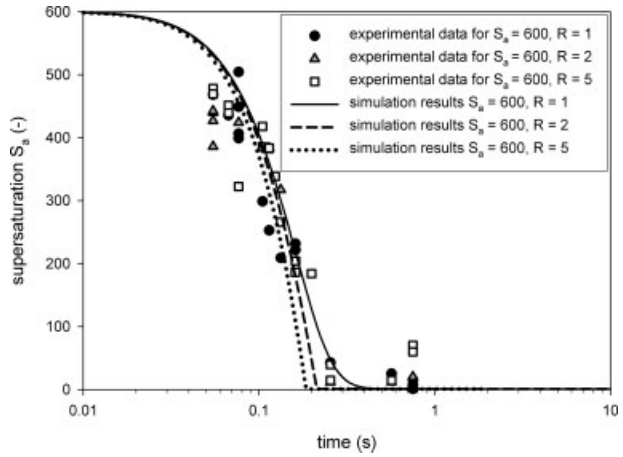

Figure 11. Depletion of supersaturation during precipitation of barium sulfate, measured *in situ* after different residence times in the tubular reactor, compared with simulation results for an initial supersaturation of S_a = 600 and various initial free lattice ion ratios (R = 1, 2, 5).

The simulation results demonstrate a high degree of correspondence with experimental results, independent of the chosen free lattice ion ratio. The only explanation for these results is that both the nucleation and growth rate are only affected by supersaturation as the thermodynamic driving force at a constant temperature of 25°C. This is even more evident when the temporal evolution of the crystalline matter in suspension is discussed (Figure 12).

Solubility equilibrium is reached after around 570 ms, independent of the free lattice ion ratio R. However, the mass at the end of the precipitation process does differ for all three ion ratios; the temporal evolution until the point that the equilibrium state is reached does not. The difference in total precipitated mass between the three initial free lattice ion ratios is due to the definition of supersaturation. The more the ion ratio deviates from stoichiometric conditions ($R = 1$), the more the mass at the end of the process is decreased. The reason for this is that (as for the formation of barium sulfate both ions are necessary in a stoichiometric ratio), in a system with an excess of barium (i.e. high R), the amount of precipitated mass is controlled by the concentration of sulfate ions.

Again all simulation curves almost perfectly fit the experimental data. This clearly indicates that at this supersaturation of $S_a = 600$, the primary processes can be described with primary kinetics consisting of nucleation and crystal growth. The investigated supersaturation is fairly close to the supersaturation of $S_a = 585$ presented by Judat and Kind,[9] recalculated from the concentration-based supersaturation of $S_c = 2500$. Judat and Kind proposed a particle formation hypothesis based on TEM and Kryo-TEM observations, which included an ordered aggregation step of nanoscale primary particles followed by a recrystallization step. This hypothesis can not be held any longer due to the fact that the simulation with experimentally obtained nucleation kinetics in combination with diffusion-controlled growth is consistent with the measured data.

Figure 12 further supports the conclusion drawn before: the nucleation and growth rate are independent of the free lattice ion ratio present during the precipitation process. The crucial parameter is supersaturation. In detail: nucleation kinetics found under stoichiometric conditions ($R = 1$) are able to describe the particle formation process under non-stoichiometric ($R \neq 1$) conditions if an adequate, activity-based supersaturation model is used to describe the thermodynamic driving force. As a reverse finding, it can be concluded that the adsorption of lattice ions, as is definitely the case for barium ions on barium sulfate particles,[19] does not influence the nucleation kinetics, which means the interfacial energy. This would imply that theoretical models, used to calculate the interfacial energy based on adsorption isotherms, would lose their physical meaning.

This finding is supported by several authors for small supersaturations: Gunn and Murthy[29] as well as Symeopoulos and Koutsoukos[30] report that the dependence of the measured induction time is only given by the educt concentrations, irrespective of the molar ratio of barium to sulfate ions. The results presented by Aoun et al.[4] contradict this: they show that nucleation and growth kinetics are slowest for stoichiometric conditions and accelerate if the ratio is either increased or decreased from this value. The explanation of the findings of Aoun et al.[4] is backed up by the fact that, for the experiments reported, only the concentration of the excess ion was changed, whereas the concentration of the ion in defect was kept constant. This means that the experiments were performed with different supersaturations and therefore thermodynamic driving forces, which definitely has to result in different nucleation as well as growth kinetics and is not the result of an acceleration effect caused by variable lattice ion ratios and therefore non-stoichiometry.

Conclusions

The particle formation process of the sparingly soluble substance barium sulfate was studied experimentally and

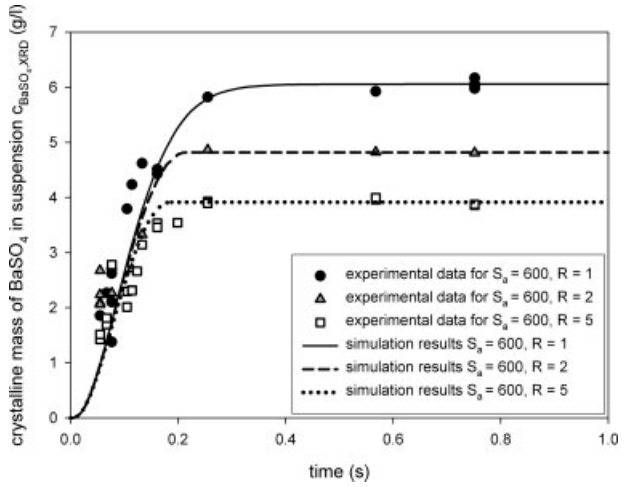

Figure 12. Comparison of crystalline mass of barium sulfate in suspension, measured *in situ* as a function of time, with simulation data for an initial supersaturation of S_a = 600 and different initial free lattice ion ratios.

numerically. The first part of the experimental section consisted of offline studies based on light-scattering and electron microscopy results. An *in situ* measuring technique is presented that allows time-resolved observations of the particle formation process of crystalline materials in timescales ranging from a few milliseconds to several seconds. A precipitation model based on the population balance equation was presented and different nucleation kinetics were tested.

The results of the offline measurements showed the presence of a heterogeneous and homogeneous nucleation region. If heterogeneous nucleation is the dominant nucleation mechanism, the particle size at the end of the process is independent of supersaturation. If the critical supersaturation is crossed and homogeneous nucleation takes control, particle size continuously decreases with increasing supersaturation.

In situ measurements showed the potential of WAXS-synchrotron radiation studies to observe particle formation processes of sparingly soluble substances on millisecond timescales. The mass fraction of crystalline barium sulfate could be detected down to values of one mass percent ($x_{BaSO_4} = 0.001$). Supersaturation and precipitated crystalline mass of barium sulfate was followed online and time-resolved between 55 and 750 ms during the solid formation process.

Furthermore, online and offline measurements support the ideas of the precipitation model presented here. The use of a proper thermodynamic model is of great importance, i.e. to describe the supersaturation in such a way that the properties of the electrolyte solution are taken into account. This was realized using an activity-based approach in combination with ion pair complex formation to calculate supersaturation. Semi-empirical nucleation kinetics in combination with diffusion-controlled crystal growth can very accurately predict the mean particle size at the end of the precipitation process as well as the temporal evolution of the particle formation process. The results presented here demonstrate that both primary formation kinetics, i.e. kinetics for nucleation and crystal growth, only depend on supersaturation as the thermodynamic driving force and do not depend on the free lattice ion ratio, which means educt ratio.

Acknowledgments

The authors gratefully thank Dr. Stephen Doyle for the support given at the WAXS beamline at the ANKA synchrotron of Forschungszentrum Karlsruhe GmbH and the Deutsche Forschungsgemeinschaft DFG for financial support.

Notation

$A_{het/hom}$ = kinetic factor in nucleation rate expression
a_i = molar activity of species i, kmol m^{-3}
B = nucleation term, m^{-4} s^{-1}
c_i = molar concentration of species i, kmol m^{-3}
D_{BaSO_4} = diffusion coefficient, m^2 s^{-1}
G = growth rate m s^{-1}
I_{BaSO_4}, I_c, I_m = integral scattered intensity
$J_{het/hom}$ = nucleation rate, m^{-3} s^{-1}
$J_{max,het/hom}$ = pre-exponential factor in nucleation rate equation, m^{-3} s^{-1}
k_B = Boltzmann constant ($1.381 \cdot 10^{-23}$), J K^{-1}
K_{ip} = ion-pair complex formation constant, kmol m^{-3}
K_{sp} = solubility product constant, kmol^2 m^6
L = particle diameter, m
L_c = size of a critical nucleus, m
$n(L)$ = particle number density of size L, m^{-4}
N = number of nuclei
q_0 = normalized number density distribution, m^{-1}
Q_0 = cumulative number density distribution
R = free lattice ion ratio
S_a = activity-based supersaturation
$S_{a,crit}$ = critical supersaturation
S_c = concentration-based supersaturation
Sh = Sherwood number
T = temperature, K
t = time, s
V_m = molecular volume, m^3 Kmol^{-1}
x_{BaSO_4} = mass fraction of barium sulfate in suspension
$x_{V,50}$ = mean (volume-weighted) particle size, m
γ_i = activity coefficient
γ_{cl} = interfacial energy, J m^{-2}
μ_m = mass absorption coefficient of mixture, m^2 kg^{-1}
ν = dissociation number
ρ_{BaSO_4} = density of barium sulfate particles, kg m^{-3}

Literature Cited

1. Nielsen AE. Homogeneous nucleation in barium sulfate precipitation. *Acta Chem Scan*. 1961;15:441–442.
2. Mohanty R, Bhandakar S, Zuromski B, Brown R, Estrin J. Characterizing the product crystals from a mixing tee process. *AIChE J*. 1988;34:2063–2068.
3. Angerhöfer M. *Untersuchung zur Kinetik der Fällungskristallisation von Bariumsulfat*. PhD Thesis. Technische Universität München, Munich, Germany, 1994.
4. Aoun M, Plasari E, David R, Villermaux J. Are barium sulphate kinetics sufficiently known for testing precipitation reactor models? *Chem Eng Sci*. 1996;51:2449–2458.
5. Fitchett D, Tarbell J. Effect of mixing on the precipitation of barium sulfate in an MSMPR reactor. *AIChE J*. 1990;36:511–522.
6. Baldyga J, Podgorska W, Pohorecki R. Mixing-precipitation model with application to double feed semi-batch precipitation. *Chem Eng Sci*. 1995;50:1281–1300.
7. Vicum L, Mazzotti M, Baldyga J. Applying a thermodynamic model to the non-stoichiometric precipitation of barium sulfate. *Chem Eng Technol*. 2003;26:325–333.
8. Schwarzer HC, Peukert W. Combined experimental/numerical study on the precipitation of nanoparticles. *AIChE J*. 2004;50:3234–3247.
9. Judat B, Kind M. Morphology and internal structure of barium sulfate—derivation of a new growth mechanism. *J Colloid Interface Sci*. 2004;269:341–353.
10. Hennessy A, Graham G, Hastings J, Siddons DP, Zhong Z. New pressure flow cell to monitor $BaSO_4$ precipitation using synchrotron in situ angle-dispersive X-ray diffraction. *J Synchrotron Rad*. 2002; 9:323–324.
11. Yoon S, Baik S, Kim MG, Shin N. Formation mechanisms of tetragonal barium titanate nanoparticles in alkoxide-hydroxide sol-precipitation synthesis. *J Am Ceram Soc*. 2006;89:1816–1821.
12. Norby P, Cahill C, Koleda S, Parise JB. A reaction cell for in situ studies of hydrothermal titration. *J Appl Crystallogr*. 1998;31:481–483.
13. Ueno S, Minato A, Yano J, Sato K. Synchrotron radiation X-ray diffraction study of polymorphic crystallization of SOS from liquid phase. *J Crystal Growth*. 1999;198:1326–1329.
14. Heeley EL, Poh CK, Li W, Maidens A, Bras W, Dolbnya IP, Gleeson AJ, Terrill NJ, Fairclough JP, Olmsted PD, Ristic RI, Hounslow MJ, Ryan AJ. Are metastable, precrystallisation, density-fluctuations a universal phenomena? *Faraday Discuss*. 2003;122:343–361.
15. MacCalman ML, Roberts KJ. Online processing of pharmaceutical materials using in situ X-ray-diffraction. *J Appl Cryst*. 1995;28:620–622.
16. Bolze J, Peng B, Dingenouts N, Panine P, Narayanan T, Ballauf M. Formation and growth of amorphous colloidal $CaCO_3$ precursor particles as detected by time-resolved SAXS. *Langmuir*. 2002;18:8364–8369.
17. Quayle MJ, Davey RJ, McDermott AJ, Tiddy GJT, Clarke DT, Jones GR. In situ monitoring of rapid crystallisation processes using synchrotron X-ray diffraction and a stopped-flow cell. *Phys Chem Chem Phys*. 2002;4:416–418.

18. Haselhuhn F, Doyle S, Kind M. Synchrotron radiation X-ray diffraction study of the particle formation of pseudo-polymorphic calcium oxalate. *J Crystal Growth*. 2006;289:727–733.
19. Kucher M, Babic D, Kind M. Precipitation of barium sulfate: experimental investigations about the influence of supersaturation and free lattice ion ratio on particle formation. *Chem Eng Process*. 2006;45: 900–907.
20. Göttlicher J, Hagelstein M. *ANKA instrumentation book*. Eggenstein-Leopoldshafen: Forschungszentrum Karlsruhe GmbH, 2006.
21. Roisnel T, Rodriguez-Carvajal J. WinPLOTR: a windows tool for powder diffraction pattern analysis. *EPDIC 7: Material Science Forum*, 2001, Volume 378–381, part 1, issue vol. 377, pp 118–123.
22. Schwarzer HC, Peukert W. Prediction of aggregation kinetics based on surface properties of nanoparticles. *Chem Eng Sci*. 2005;60:11–25.
23. Monnin C. A thermodynamic model for the solubility of barite and celestite in electrolyte solutions and seawater to 200°C and to 1 kbar. *Chem Geol*. 1999;153:187–209.
24. Bromley LA. Thermodynamic properties of strong electrolytes in aqueous solution. *AIChE J*. 1973;19:313–320.
25. Mersmann A. *Crystallization Technology Handbook*. New York: Marcel Dekker, 1995.
26. Roelands CPM, Ter Horst JH, Kramer HJM, Jansens PJ. Analysis of nucleation rate measurements in precipitation processes. *Cryst Growth Des*. 2006;6:1380–1392.
27. Nielsen AE. Nucleation and growth of crystals at high supersaturations. *Kristall und Technik*. 1969;4:17–38.
28. Söhnel O, Garside J. *Precipitation, Basic principles and Industrial Application*. Oxford: Buttersworth-Heinemann, 1992.
29. Gunn J, Murthy MS. Kinetics and mechanisms of precipitations. *Chem Eng Sci*. 1972;27:1293–1313.
30. Symeopoulos B, Koutsoukos P. Spontaneous precipitation of barium sulfate in aqueous solution. *J Chem Faraday Trans*. 1992;88:3063–3066.

Manuscript received Aug. 28, 2007, revision received Nov. 12, 2007, and final revision received Jan. 15, 2008.